

2020-10

In situ AFM-based nanoscale rheology reveals regional non-uniformity in viscoporoelastic mechanical behavior of the murine periodontal ligament

B.K. Connizzo, G.R.S. Naveh. 2020. "In situ AFM-based nanoscale rheology reveals regional non-uniformity in viscoporoelastic mechanical behavior of the murine periodontal ligament." *Journal of Biomechanics*, Volume 111, pp. 109996 - 109996. <https://doi.org/10.1016/j.jbiomech.2020.109996>
<https://hdl.handle.net/2144/43218>

"Downloaded from OpenBU. Boston University's institutional repository."



HHS Public Access

Author manuscript

J Biomech. Author manuscript; available in PMC 2021 October 09.

Published in final edited form as:

J Biomech. 2020 October 09; 111: 109996. doi:10.1016/j.jbiomech.2020.109996.

In Situ AFM-Based Nanoscale Rheology Reveals Regional Non-Uniformity in Viscoporoelastic Mechanical Behavior of the Murine Periodontal Ligament

Brianne K. Connizzo¹, Gili R. S. Naveh²

¹Department of Biological Engineering, Massachusetts Institute of Technology, Cambridge, MA 02139, United States

²Department of Oral Medicine, Infection and Immunity, School of Dental Medicine, Harvard University, Boston, MA 02115, United States

Abstract

The periodontal ligament (PDL) is a critical player in the maintenance of tooth health, acting as the primary stabilizer of tooth position. Recent studies have identified two unique regions within the PDL, the ‘dense collar’ region and the ‘furcation’ region, which exhibit distinct structural and compositional differences. However, specific functional differences between these regions have yet to be investigated. We adapted an AFM-based nanoscale rheology method to regionally assess mechanical properties and poroelasticity in the mouse PDL while minimizing the disruption of the 3-dimensional native boundary conditions, and then explored tissue mechanical function in four different regions within the dense collar as well as in the furcation region. We found significant differences between the collar and furcation regions, with the collar acting as a stabilizing ligamentous structure and the furcation acting as both a compressive cushion for vertical forces and a conduit for nutrient transport. While this finding supports our hypothesis, based on previous studies investigating structural and compositional differences, we also found surprising inhomogeneity within the collar region itself. This inhomogeneity supports previous findings of a tilting movement in the buccal direction of mandibular molar teeth and the structural adaptation to prevent lingual movement. Future work will aim to understand how different regions of the PDL change functionally during biological or mechanical perturbations, such as orthodontic tooth movement, development, or aging, with the ultimate goal of better understanding the mechanobiology of the PDL function in health and disease.

Keywords

periodontal ligament; mechanics; poroelasticity; viscoelasticity; AFM

Correspondence: Brianne K. Connizzo, 70 Massachusetts Avenue, NE47-377, Cambridge, MA 02139, T: 617-253-2469, connizzo@mit.edu.

Author Contributions Statement: BK Connizzo and GRS Naveh have contributed to all aspects of this study, including research design, data acquisition, interpretation/analysis of data, and drafting/revision of the manuscript. All authors have read and approved the final submitted manuscript.

Conflict of Interest Statement

There are no known conflicts of interest associated with this publication or any of its authors and there has been no significant financial support for this work that could have influenced its outcome.

Introduction

The periodontal ligament (PDL) is a complex soft-tissue that is situated between the tooth and the jaw bone (Berkovitz, 1990; Nanci and Bosshardt, 2006). Like other ligaments, the PDL is composed of collagens (I, III, IV, V, VI, XII, XIV) with type I collagen in highest abundance, non-collagenous proteins, such as proteoglycans and their associated glycosaminoglycans (GAGs), and a cellular component composed of mainly fibroblasts. The collagen structure of the PDL is of particular interest as organization and strength of the collagen structure is critical to ligament mechanical function. In general, collagen fibers span between the bone and tooth cementum forming two unique load-bearing attachment sites that dissipate loads throughout the bone (Lee et al., 2015). The collagen network along the root is oriented in longitudinal sheets with the inner fibers oriented perpendicular to the long axis of the tooth, but slightly angled towards the apical surface. This direction alludes to its primary function in restricting downward tooth movement during chewing (Nanci, 2017; Naveh et al., 2018). Despite being labeled as a continuous structure, recent studies have shown that the PDL has several distinct regions of collagen networks that are correlated with tissue function (Naveh et al., 2018, 2013; Nikolaus et al., 2017). Specifically, there exists a dense network of collagen fibers near the gum line that surrounds the entire tooth, termed the ‘dense collar’ region, and a sparser network of collagen fibers near the junction of the two roots, termed the ‘furcation’ region. The relationship between these different networks and the mechanical function of the PDL has yet to be explored.

Due to their lack of regenerative capacity, teeth rely on the ability to move and deform in order to prevent stress concentrations and structural damage to the tooth, which is especially important under the high repetitive loads during mastication. The PDL is a critical player in the maintenance of tooth health, acting as the primary stabilizer of tooth position by dissipating and transferring loads to the underlying alveolar bone guided by everyday functional demands. In tension, the PDL exhibits characteristically ligamentous mechanical behavior with a non-linear stress-strain curve and rate-dependent behavior (Bergomi et al., 2010; Dorow et al., 2003; Pini et al., 2004; Rees and Jacobsen, 1997; Toms et al., 2002; Wu et al., 2018). Few studies have observed self-stiffening and poroelasticity (Oskui et al., 2016; van Driel et al., 2000), but none of these have directly measured the dynamic nanoscale behavior of the PDL while preserving the 3D context of the tissue. Instead, PDL dynamic function has been modeled using constitutive and finite element models addressing the PDL as a uniform tissue (Huang et al., 2017; Natali et al., 2008; Nikolaus et al., 2017; Oskui et al., 2016; Oskui and Hashemi, 2016; van Driel et al., 2000). This behavior has been tested in multiple teeth, multiple root levels, and multiple animal models, yielding a wide variety of results (elastic moduli ranging from 0.07MPa to 1750MPa) thus indicating tissue non-uniformity. Recent studies demonstrated that teeth present a preferred trajectory of movement (Chattah et al., 2009; Naveh et al., 2018, 2012; Salamati et al., 2020), which further support the 3D inhomogeneity. Despite this, there is still much uncertainty regarding regional mechanical behavior. While the periodontal ligament is exposed to many different types of loading, mechanical function has mostly been studied in uniaxial quasi-static tension. In addition, certain regions of the PDL, such as the furcation, and differences along the collar within a certain root level have never been explored.

Therefore, the objective of this study was two-fold: (1) to develop a method to regionally assess tissue mechanical properties and poroelasticity in the mouse periodontal ligament minimizing the disruption of the 3D structure and natural boundary conditions of the tissue, and (2) to explore the regional heterogeneity in PDL properties as it relates to the dense collar and furcation regions. We hypothesized first that the mouse PDL would exhibit nanomechanical properties similar to other tendons/ligaments, exhibiting independent visco- and poroelastic properties. We also hypothesized that the furcation region would be softer than the dense collar region, and that there would be buccal-lingual inhomogeneity due to the tooth trajectory during mastication.

Methods

All animal experiments were approved and performed in compliance with NIH's Guide for the Care and Use of Laboratory Animals and guidelines from the Harvard University Institutional Animal Care and Use Committee (Protocol No. 01840).

Sample Preparation

Thirteen male C57BL/6 mice at 9 weeks of age were sacrificed and their mandibles were dissected, cleaned from extraneous tissue, and split into hemi-mandibles through the fibrous symphysis (Fig. 1A). Hemi-mandibles were immediately embedded in SCEM embedding material (Section-lab, Japan) followed by snap freezing in 2 methyl-butane cooled with liquid nitrogen. Samples were then mounted on a cryostat and sectioned from apical region in the transverse plane to remove tissue until the level of the furcation (Fig. 1B). All samples were then stored at -80°C until mechanical testing. On the day of testing, samples were thawed in distilled water to dissolve cryosectioning medium and then transferred to phosphate-buffered saline (1x PBS) for the remainder of sample preparation. First, regions of interest were identified under a light microscope and Verhoeff's tissue stain was applied to the pulp of each root for accurate identification under AFM optics. The dimensions of each tooth were then measured from sample images using ImageJ (Rueden et al., 2017), which allowed for repeatable unbiased definition of starting points for each series of indentations. Samples were then bonded to a custom stage for testing using a dental restorative composite material (Fig. 1C), Z100™ (3M ESPE, St. Paul, MN) and indentations were performed on the cross-section (Fig. 1D). All samples were kept hydrated with PBS for the duration of the experiments.

High-frequency AFM-based Rheology System

For regional nanoscale evaluation, indentations were performed at twenty-nine regions in five series to indent the collar region in four locations (mesial-lingual, mesial-buccal, distal-lingual, distal-buccal), as well as within the furcation region (Fig. 2A). Built-in top-view optics (10x objective) and x-y translational stage (accuracy $\sim 5\mu\text{m}$) were used to visualize positions of locations throughout the testing procedure. This indentation protocol was developed due to the small size of the murine PDL and the lack of direct visualization on our low magnification AFM-based system, such that 1–2 indentation positions within a regional series would definitively indent PDL tissue. The first series of indentations was defined as 85% of the distance from pulp to tooth-edge towards the lingual surface of the distal root.

We then performed six indentations every 50 μm moving in the lingual direction ('DL', p1–6). The next six indentations were performed in the opposite direction, indenting every 50 μm surface beginning at 85% of the distance from root to tooth-edge in the buccal direction ('DB', p7–12). Seven indentations were performed in the furcation region, where the first indentation was defined as 85% of the distance from the distal root pulp center to the tooth edge moving towards the mesial root ('F', p13–19). We then repeated the lingual-buccal procedure on the mesial root for the remaining indentations ('ML', p20–24; 'MB', p25–29) with 5 indentations in each region due to anatomical differences in size.

For each indentation, our custom high-frequency rheology system was used to measure the complex modulus of samples over a wide frequency range (1 Hz to 10 kHz), allowing for measurement under variable loading rate (Azadi et al., 2016; Connizzo and Grodzinsky, 2017b; Nia et al., 2013; Oftadeh et al., 2018). For all experiments, polystyrene colloidal probe tips with 25 μm diameter (Polysciences, Warrington, PA) were attached to tipless cantilevers (Budget Sensors, Sofia, Bulgaria) by the lift-off process. This probe size was previously shown to provide the best visualization of the two-peak phase response in ligamentous tissues, allowing us to independently analyze the two peaks. The nominal spring constant of all cantilevers used was $k \sim 7.4 \text{ N/m}$ but spring constant was directly measured for each tip using the thermal calibration method (Hutter and Bechhoefer, 1993).

The indentation loading profile consisted of an initial load-controlled ramp-and-hold pre-indentation of approximately $\sim 0.5\text{--}4 \mu\text{m}$. This study did not include any preconditioning of the tissue. Nanoscale dynamic tests are superimposed on top of a microscale indentation once the tissue has fully relaxed, which ensures that each region tested is in direct contact with the probe and pre-loaded. Dynamic tests are performed using a random binary sequence (RBS) with displacements of 8–12nm, which allows us to reduce signal-to-noise ratio and experimental time when using a wide-bandwidth frequency generator. (Connizzo and Grodzinsky, 2017a; Nia et al., 2013). Briefly, we applied a low-pass filter and then a sign operator ($\text{sign}(x) = 1$ for $x \geq 0$ and $\text{sign}(x) = -1$ for $x < 0$) to simulated white Gaussian noise and generate the RBS. The amplitude of the resulting dataset was then scaled to the maximum allowable excitation given to the secondary piezo actuator. The sampling rate was set to $f_s = 100 \text{ kHz}$ with the length of $T = 30 \text{ s}$ and cut-off frequency set at $f_c = 1 \text{ Hz}$. Data processing was then performed in MATLAB (The MathWorks, Natick, MA) as described previously (Connizzo and Grodzinsky, 2017a; Nia et al., 2013; Oftadeh et al., 2018). A discrete Fourier transform was used to obtain the fundamental frequency component of the dynamic force F_{OSC} and displacement δ signals, which then allowed us to calculate the magnitude and phase of the dynamic complex modulus at each frequency. All dynamic tests are performed three times in each location and averaged to ensure a consistent response.

Data Analysis

The effective indentation modulus was computed using a Hertzian contact mechanics model as previously described (Han et al., 2011). From the magnitude and phase curves of the dynamic modulus, we then define and calculate seven different parameters (Fig. 2B). We identify the location of the viscoelastic and poroelastic peaks as the first and second peaks, respectively, in the two-peak phase response (termed viscoporoelastic behavior). We then

identify the frequency (f_v , f_p) and phase angle (δ_v , δ_p) at which each peak occurs. The low frequency modulus (E_L) is the magnitude at the initial frequency while the high frequency modulus (E_H) is the magnitude at the frequency 4x higher than the peak poroelastic frequency. Finally, we calculate the tissue self-stiffening ratio (E_H/E_L) (Nia et al., 2015).

For each of the twenty-nine different regions, indentations were performed three times and data were averaged to ensure a consistent response. Each indentation was then identified as bone-like, cartilage-like or ligament-like based on a series of criteria as follows (Fig. 3A). ‘Bone-like’ regions were high moduli regions with low phase shift ($<5^\circ$). ‘Cartilage-like’ regions were identified by a single poroelastic peak in the phase angle response, along with larger self-stiffening ratios. Finally, ‘ligament-like’ regions were low moduli regions with a characteristic two-peak phase response. We identified which regions had mostly ligament-like indentations over all PDL samples and chose 2–4 regions for each anatomical location (Fig. 3B). All indentations that were identified as ‘bone-like’ or ‘cartilage-like’, even within those 2–4 chosen regions, were excluded from PDL statistical analyses to identify specific regions that were in the midsubstance of the PDL. Some of the cartilage-like regions may be part of the PDL attachment to the adjacent bone or tooth, but this was beyond the scope of this initial investigation and we plan to explore them more closely in the future.

Statistical Analysis

For all data within a certain anatomical location, it was determined via Mann-Whitney test that the variance within a single specimen was not different from the variance between specimens. Therefore, data from all indentations across the thirteen mice tested were considered as individual data points for each region resulting in a variable sample size of 12–34 indentations. Statistical comparisons were then made for each mechanical parameter using a non-parametric one-way ANOVA (Kruskal-Wallis test) with Dunns post-hoc tests for specific comparisons between anatomical regions. Significance was set at $p < 0.05$ and is marked by lines between compared groups on all figures, where a solid black line represents comparisons with the furcation, a dashed orange line represents lingual-buccal comparisons, and a dotted yellow line represents distal-mesial comparisons.

Results and Discussion

We report here for the first time the regional mechanical properties of the PDL in an *in-situ* model. More specifically, direct experimental data regarding the visco- and poroelastic dynamic mechanical properties of the mouse PDL were obtained without disrupting the native boundary conditions of the ligament. Through this process, we were able to identify and distinguish at least three different types of mechanical behavior within the tooth-PDL-bone complex, which was attributed to three tissue types. Ligament-like and cartilage-like regions were similar to previously described data (Connizzo and Grodzinsky, 2017b; Nia et al., 2011) for mouse supraspinatus tendon and bovine articular cartilage, respectively. This was, however, the first time our nanoscale rheology has been used to indent bone-like tissue, and the data are consistent with what would be expected for stiff mineralized tissue, exhibiting more elastic behavior with high compressive moduli values. However, this ‘bone-like’ group likely includes alveolar bone and tooth (dentin, cementum) so future studies

would be necessary to further characterize these individual tissues which was outside the scope of the present work. More importantly, this work focuses on the changes found in PDL which was determined to be vastly more inhomogeneous than we expected. We report here mechanical properties of the furcation region for the first time and identify significant non-uniformity within the dense collar region that mimic native PDL loading.

The dense collar, particularly in the distal buccal region, had increased modulus compared to the furcation region (Fig. 4A–C). Compared to the furcation region, the distal buccal region exhibited a 6-fold higher microscale indentation modulus (95 ± 106 vs. 16 ± 17 kPa) and similar increases in low and high frequency moduli. This suggests that the furcation region is softer or more compressible than the collar region. We propose that the dense collar functions to suspend the tooth within the bone socket and prevent significant translational and rotational movements during mastication. This explains why the collar exhibits a dense collagen network orientated horizontally (Hirashima et al., 2019; Lee et al., 2015; Naveh et al., 2018, 2012). In contrast, the furcation (Ben-Zvi et al., 2019, p.; Maria et al., 2019; Naveh et al., 2018, 2012) is compressed with high mastication forces, potentially acting more as a space filler. In fact, previous studies have shown a less dense collagen network and increased vasculature in the furcation region compared to in the dense collar (Naveh et al., 2018, 2012). While the furcation exhibited the lowest moduli values with low frequency or quasi-static loading, it also had high self-stiffening ratios and increased poroelastic behavior, leaning more towards cartilage-like behavior at high frequencies. In fact, the largest percentage of ‘cartilage-like’ regions were found when probing for the furcation (Fig. 3B). Specific methodologies used here prevent us from identifying whether these cartilage-like regions are part of the PDL proper or part of the attachment to other tissues (as in other tendons/ligaments), but we hypothesize that this region exhibits properties of both ligament and cartilage and subsequently has dual function. It provides space for the tooth to move vertically with increased compressibility while preventing tooth movement in the other directions through its sparse network of collagen fibers. It also functions to allow load transfer to the alveolar bone rather than the cortical bone which has a low remodeling capacity.

We also found asymmetry with respect to tissue modulus within the collar itself in both the distal and mesial roots of the tooth (Fig. 4B,C, Fig. 6). The buccal regions had approximately 3-fold higher moduli compared to the lingual counterparts (55 ± 7 vs. 16 ± 1 kPa for mesial and 63 ± 6 vs. 23 ± 2 kPa for distal in low frequency modulus, for example), suggesting restricted movement in the buccal direction. When looking at the morphology of grinding teeth (molar, premolar), the long axes of the crown and root are angled such that vertical loading of the tooth along the crown axis will cause the tooth to crush against the buccal side. Therefore, vertical forces applied to the tooth will generate higher compression in the buccal PDL due to the relative rotation of the tooth. Resistance to compressibility, which is relevant for both direct compressive loading as well as lateral compression due to tensile stress (Poisson effects), therefore would also likely be higher in the buccal region. This loading pattern of compressing the buccal bone was indeed showed in studies simulating mastication loads and associated tooth movement (Naveh et al., 2018, 2012; Nikolaus et al., 2017; Salamati et al., 2020). This is probably the reason for the higher vertical dimension of the buccal alveolar bone relative to the lingual side.

Interestingly, we also found non-uniformity across collar regions with respect to tissue self-stiffening (Fig. 4D, Fig. 6). Within the collar, self-stiffening ratios were highest in the distal-buccal and mesial-lingual regions and lowest in the mesial-buccal and distal-lingual regions. The self-stiffening ratio relates to the ability of tissue to pressurize and stiffen with higher frequency dynamic loading. We hypothesize this could be adaptation to prevent tooth rotation due to shear and torque forces caused by high frequency grinding and tearing movements. However, relationships between these four regions of the PDL may be specific to this tooth position as the majority of grinding does occur at the molars and it was previously shown that PDL mechanical properties might vary dramatically based on tooth type (Pini et al., 2004). Furthermore, this work focuses on a single tooth that has only one neighboring tooth on the distal side. Regardless, these differences allude to the resistance to complex loading in the molars involving multiple types, durations, and frequencies of loading during mastication. Interestingly, the furcation also had a higher self-stiffening ratio than the distal-lingual and mesial-buccal regions (Fig. 4D). The presence of higher self-stiffening in the furcation could be indicative of a more cushion-like function in this region, or just an association with preventing deformation during high frequency and high magnitude chewing events.

In addition to changes in tissue modulus, a number of significant differences were found in the poroelastic behavior of the PDL. Poroelastic peak phase angle and frequency were highest in the furcation, distal- and mesial-lingual regions and lowest in the distal- and mesial-buccal regions (Fig. 5A,B). Since poroelastic peak frequency is associated with fluid flow, we can attribute these changes primarily to differences in tissue permeability. Using the peak frequency and low frequency modulus, we can estimate the permeability of each of the regions, which ranged from 10^{-14} to 10^{-15} $\text{m}^4/\text{N}\cdot\text{s}$, and compare the relative values amongst the five regions measured (Fig. 6). The values for all of the PDL regions were lower than that of mouse supraspinatus tendon, which has been reported to be around 10^{-13} $\text{m}^4/\text{N}\cdot\text{s}$ (Oftadeh and Grodzinsky, 2017), but higher than or similar to that of bovine articular cartilage, which has been reported in the range of 10^{-15} $\text{m}^4/\text{N}\cdot\text{s}$ (Nia et al., 2011). The furcation region had both high self-stiffening and high permeability, suggesting a tissue that must pressurize quickly to withstand dynamic high frequency loads but also allow for that fluid to exude swiftly and not become trapped inside the matrix network. This could be explained by the lack of large proteoglycans such as in cartilage and intervertebral disc which effectively trap fluid inside the tissue (Azadi et al., 2016; Nia et al., 2015). Previous studies have also shown that large blood vessels are also present the furcation region (Naveh et al., 2018), which could explain the need for high permeability in relation to nutrient transport.

Interestingly, we did not find many changes in the viscoelastic properties of the PDL (Fig. 5C,D). The viscoelastic peak phase angle was increased in the furcation compared to both distal regions, and the mesial-lingual region exhibited higher viscoelastic phase compared to the distal-lingual region. The viscoelastic peak is generally attributed to inherent viscoelastic properties of the tissue structure itself or dynamic interactions within the structure, such sliding/re-organization of the collagen fibrils. It's still unclear what differences in the phase angle of the viscoelastic peak signify physically, but since the viscoelastic phase angle increases with higher fibrillar modulus (Oftadeh et al., 2018), we speculate it may relate to

the density or organization of collagen fibrils. We do know that the viscoelastic frequency is inversely proportional to the relaxation time of the tissue and there does not appear to be any significant differences between groups in this parameter.

A few recent studies have also investigated compressive function in human PDL demonstrating vast heterogeneity within and between specimens as well as directionally-dependent viscoelastic behavior (Najafidoust et al., 2020; Wu et al., 2020), but these studies were performed by indenting along the long axis of the PDL rather than in the transverse direction as in this study. Regardless, dynamic testing pointed to a dominance of interstitial fluid flow in the mechanical response, similar to that of a biphasic material like articular cartilage and to what we have reported. While our method focuses on nanoscale transverse compression, fluid flow and permeability measures are relevant for all directions and therefore this work is relevant for overall mechanical function. Furthermore, this method may be a good model for fluid exudation in tension due to Poisson effects, particularly in a highly anisotropic tissue. Recent studies investigating dynamic tensile function have also demonstrated heterogeneity in PDL viscoelastic properties with root level but not between mesial and distal surfaces (Uhlir et al., 2017; Wu et al., 2019, 2018). Our data consistently also showed limited differences between the mesial and distal surfaces, but instead demonstrated large variability in bucco-lingual properties, which to our knowledge has not been measured in previous studies.

While this study presents a novel method of measuring the nanomechanical properties of the mouse PDL, it is not without limitations. Within this experiment, there is a high variability of tissue properties within and between specimens. We believe some of this is due to difficulties in sectioning, both obtaining samples sectioned to the same root level as well as obtaining the correct plane of sectioning, but our results also demonstrate heterogeneity within the PDL itself. In addition, we only separated samples based on whether they fell into 'bone-like', 'cartilage-like', or 'ligament-like' tissue due to our knowledge of dynamic behavior in musculoskeletal tissues. These exclusion criteria were defined based on our indentation protocol, which was designed to indent each region over six locations spanning from bone to tooth to provide consistency across samples with varying PDL widths. However, this also introduces some inherent bias in the results, particularly as some cartilage-like regions may be considered part of the PDL midsubstance and contributing to the non-uniformity. Alternatively, this could also be the insertion of the PDL into adjacent bone or tooth which was not within the scope of this study. High resolution imaging methods are required to thoroughly investigate this and will be explored in future studies. Furthermore, there are many different biological tissues that have not been assessed using this rheological technique and could exhibit similar dynamic properties, such as blood vessels, skin, fat, etc. This is particularly important for the furcation region, since vasculature could be interacting with our analyses and would be difficult to identify using current optical techniques.

This work for the first time reports on the regionally-specific mechanical properties within the PDL, providing mechanical evidence to the role of the furcation in withstanding compressive forces and the role of the collar in limiting translation and rotation of the tooth. While we expected to find differences between the collar and furcation regions, we found

surprising inhomogeneity within the collar region itself. This inhomogeneity supports previous findings of a tilting movement in the buccal direction of mandibular molar teeth and the structural adaptation to prevent such movement. Future work will aim to understand how different parts of the PDL structure and mechanical function change during biological or mechanical perturbations, such as orthodontic tooth movement, development, or aging, with the ultimate goal of better understanding the mechanobiology of the PDL function in health and disease, as well as opening new avenues for the development of regenerative therapies.

Acknowledgements

This study was supported by the NIH (NIA K99-AG063896, PI:Connizzo; NIDCR R00DE025053, PI:Naveh) and the NSF (CMMI-1536233; Co-I:Grodzinsky). We would also like to acknowledge Dr. Alan J. Grodzinsky for his contributions to this work. Figures 1, 2A, and 6 were created with [Biorender.com](https://biorender.com).

References

- Azadi M, Nia HT, Gauci SJ, Ortiz C, Fosang AJ, Grodzinsky AJ, 2016 Wide bandwidth nanomechanical assessment of murine cartilage reveals protection of aggrecan knock-in mice from joint-overuse. *J. Biomech* 49, 1634–1640. 10.1016/j.jbiomech.2016.03.055 [PubMed: 27086115]
- Ben-Zvi Y, Maria R, Pierantoni M, Brumfeld V, Shahar R, Weiner S, 2019 Response of the tooth-periodontal ligament-bone complex to load: A microCT study of the minipig molar. *J. Struct. Biol* 205, 155–162. 10.1016/j.jsb.2019.01.002 [PubMed: 30639926]
- Bergomi M, Wiskott HWA, Botsis J, Mellal A, Belser UC, 2010 Load response of periodontal ligament: assessment of fluid flow, compressibility, and effect of pore pressure. *J. Biomech. Eng* 132, 014504 10.1115/1.4000154 [PubMed: 20524752]
- Berkovitz BKB, 1990 The structure of the periodontal ligament: an update. *Eur. J. Orthod* 12, 51–76. 10.1093/ejo/12.1.51 [PubMed: 2180728]
- Chattah NL-T, Shahar R, Weiner S, 2009 Design Strategy of Minipig Molars Using Electronic Speckle Pattern Interferometry: Comparison of Deformation under Load between the Tooth-Mandible Complex and the Isolated Tooth. *Adv. Mater* 21, 413–418. 10.1002/adma.200801187
- Connizzo BK, Grodzinsky A, 2017a Multiscale Poroviscoelastic Compressive Properties of Mouse Supraspinatus Tendons Are Altered in Young and Aged Mice. *J. Biomech. Eng* 10.1115/1.4038745
- Connizzo BK, Grodzinsky AJ, 2017b Tendon exhibits complex poroelastic behavior at the nanoscale as revealed by high-frequency AFM-based rheology. *J. Biomech* 54, 11–18. 10.1016/j.jbiomech.2017.01.029 [PubMed: 28233551]
- Dorow C, Krstin N, Sander F-G, 2003 Determination of the mechanical properties of the periodontal ligament in a uniaxial tensional experiment. *J. Orofac. Orthop. Fortschritte Kieferorthopadie OrganOfficial J. Dtsch. Ges. Kieferorthopadie* 64, 100–107. 10.1007/s00056-003-0225-7
- Han L, Frank EH, Greene JJ, Lee H-Y, Hung H-HK, Grodzinsky AJ, Ortiz C, 2011 Time-dependent nanomechanics of cartilage. *Biophys. J* 100, 1846–1854. 10.1016/j.bpj.2011.02.031 [PubMed: 21463599]
- Hirashima S, Ohta K, Kanazawa T, Togo A, Kakuma T, Kusukawa J, Nakamura K-I, 2019 Three-dimensional ultrastructural and histomorphological analysis of the periodontal ligament with occlusal hypofunction via focused ion beam/scanning electron microscope tomography. *Sci. Rep* 9, 9520 10.1038/s41598-019-45963-w [PubMed: 31266989]
- Huang H, Tang W, Tan Q, Yan B, 2017 Development and parameter identification of a visco-hyperelastic model for the periodontal ligament. *J. Mech. Behav. Biomed. Mater* 68, 210–215. 10.1016/j.jmbbm.2017.01.035 [PubMed: 28187321]
- Hutter JL, Bechhoefer J, 1993 Calibration of atomic-force microscope tips. *Rev. Sci. Instrum* 64, 1868–1873. 10.1063/1.1143970

- Lee J-H, Pryce BA, Schweitzer R, Ryder MI, Ho SP, 2015 Differentiating zones at periodontal ligament-bone and periodontal ligament-cementum entheses. *J. Periodontal Res* 50, 870–880. 10.1111/jre.12281 [PubMed: 26031604]
- Maria R, Ben-Zvi Y, Rechav K, Klein E, Shahar R, Weiner S, 2019 An unusual disordered alveolar bone material in the upper furcation region of minipig mandibles: A 3D hierarchical structural study. *J. Struct. Biol* 206, 128–137. 10.1016/j.jsb.2019.02.010 [PubMed: 30849471]
- Najafidoust M, Hashemi A, Oskui IZ, 2020 Dynamic viscoelastic behavior of bovine periodontal ligament in compression. *J. Periodontal Res* 10.1111/jre.12751
- Nanci A, 2017 *Ten Cate's Oral Histology: Development, Structure, and Function*, 9th ed Elsevier Health Sciences.
- Nanci A, Bosshardt DD, 2006 Structure of periodontal tissues in health and disease*. *Periodontol.* 2000 40, 11–28. 10.1111/j.1600-0757.2005.00141.x
- Natali AN, Carniel EL, Pavan PG, Sander FG, Dorow C, Geiger M, 2008 A visco-hyperelastic-damage constitutive model for the analysis of the biomechanical response of the periodontal ligament. *J. Biomech. Eng* 130, 031004 10.1115/1.2900415 [PubMed: 18532853]
- Naveh GRS, Brumfeld V, Shahar R, Weiner S, 2013 Tooth periodontal ligament: Direct 3D microCT visualization of the collagen network and how the network changes when the tooth is loaded. *J. Struct. Biol* 181, 108–115. 10.1016/j.jsb.2012.10.008 [PubMed: 23110851]
- Naveh GRS, Foster JE, Silva Santisteban TM, Yang X, Olsen BR, 2018 Nonuniformity in ligaments is a structural strategy for optimizing functionality. *Proc. Natl. Acad. Sci. U. S. A* 115, 9008–9013. 10.1073/pnas.1807324115 [PubMed: 30126991]
- Naveh GRS, Shahar R, Brumfeld V, Weiner S, 2012 Tooth movements are guided by specific contact areas between the tooth root and the jaw bone: A dynamic 3D microCT study of the rat molar. *J. Struct. Biol* 177, 477–483. 10.1016/j.jsb.2011.11.019 [PubMed: 22138090]
- Nia HT, Bozchalooi IS, Li Y, Han L, Hung H-H, Frank E, Youcef-Toumi K, Ortiz C, Grodzinsky A, 2013 High-bandwidth AFM-based rheology reveals that cartilage is most sensitive to high loading rates at early stages of impairment. *Biophys. J* 104, 1529–1537. 10.1016/j.bpj.2013.02.048 [PubMed: 23561529]
- Nia HT, Han L, Bozchalooi IS, Roughley P, Youcef-Toumi K, Grodzinsky AJ, Ortiz C, 2015 Aggrecan nanoscale solid-fluid interactions are a primary determinant of cartilage dynamic mechanical properties. *ACS Nano* 9, 2614–2625. 10.1021/nn5062707 [PubMed: 25758717]
- Nia HT, Han L, Li Y, Ortiz C, Grodzinsky A, 2011 Poroelasticity of cartilage at the nanoscale. *Biophys. J* 101, 2304–2313. 10.1016/j.bpj.2011.09.011 [PubMed: 22067171]
- Nikolaus A, Currey JD, Lindtner T, Fleck C, Zaslansky P, 2017 Importance of the variable periodontal ligament geometry for whole tooth mechanical function: A validated numerical study. *J. Mech. Behav. Biomed. Mater* 67, 61–73. 10.1016/j.jmbbm.2016.11.020 [PubMed: 27987427]
- Oftadeh R, Connizzo BK, Nia HT, Ortiz C, Grodzinsky AJ, 2018 Biological connective tissues exhibit viscoelastic and poroelastic behavior at different frequency regimes: Application to tendon and skin biophysics. *Acta Biomater.* 70, 249–259. 10.1016/j.actbio.2018.01.041 [PubMed: 29425716]
- Oftadeh R, Grodzinsky AJ, 2017 Biological Tissues Show Poroelastic and Viscoelastic Behaviour at Different Frequency Spectrums. Presented at the Summer Bioengineering, Biotransport, and Biomechanics Conference, Tucson, AZ.
- Oskui IZ, Hashemi A, 2016 Dynamic tensile properties of bovine periodontal ligament: A nonlinear viscoelastic model. *J. Biomech* 49, 756–764. 10.1016/j.jbiomech.2016.02.020 [PubMed: 26920510]
- Oskui IZ, Hashemi A, Jafarzadeh H, 2016 Biomechanical behavior of bovine periodontal ligament: Experimental tests and constitutive model. *J. Mech. Behav. Biomed. Mater* 62, 599–606. 10.1016/j.jmbbm.2016.05.036 [PubMed: 27315371]
- Pini M, Zysset P, Botsis J, Contro R, 2004 Tensile and compressive behaviour of the bovine periodontal ligament. *J. Biomech* 37, 111–119. 10.1016/s0021-9290(03)00234-3 [PubMed: 14672574]
- Rees JS, Jacobsen PH, 1997 Elastic modulus of the periodontal ligament. *Biomaterials* 18, 995–999. 10.1016/s0142-9612(97)00021-5 [PubMed: 9212195]

- Rueden CT, Schindelin J, Hiner MC, DeZonia BE, Walter AE, Arena ET, Eliceiri KW, 2017 ImageJ2: ImageJ for the next generation of scientific image data. *BMC Bioinformatics* 18, 529 10.1186/s12859-017-1934-z [PubMed: 29187165]
- Salamati A, Chen J, Herring SW, Liu Z-J, 2020 Functional tooth mobility in young pigs. *J. Biomech* 104, 109716 10.1016/j.jbiomech.2020.109716 [PubMed: 32173029]
- Toms SR, Dakin GJ, Lemons JE, Eberhardt AW, 2002 Quasi-linear viscoelastic behavior of the human periodontal ligament. *J. Biomech* 35, 1411–1415. 10.1016/s0021-9290(02)00166-5 [PubMed: 12231287]
- Uhlir R, Mayo V, Lin PH, Chen S, Lee Y-T, Hershey G, Lin F-C, Ko C-C, 2017 Biomechanical characterization of the periodontal ligament: Orthodontic tooth movement. *Angle Orthod.* 87, 183–192. 10.2319/092615-651.1 [PubMed: 27542105]
- van Driel WD, van Leeuwen EJ, Von den Hoff JW, Maltha JC, Kuijpers-Jagtman AM, 2000 Time-dependent mechanical behaviour of the periodontal ligament. *Proc. Inst. Mech. Eng. [H]* 214, 497–504. 10.1243/0954411001535525
- Wu B, Fu Y, Shi H, Yan B, Lu R, Ma S, Markert B, 2018 Tensile testing of the mechanical behavior of the human periodontal ligament. *Biomed. Eng. Online* 17, 172 10.1186/s12938-018-0607-0 [PubMed: 30470224]
- Wu B, Pu P, Zhao S, Izadikhah I, Shi H, Liu M, Lu R, Yan B, Ma S, Markert B, 2020 Frequency-related viscoelastic properties of the human incisor periodontal ligament under dynamic compressive loading. *PloS One* 15, e0235822 10.1371/journal.pone.0235822 [PubMed: 32658896]
- Wu B, Zhao S, Shi H, Lu R, Yan B, Ma S, Markert B, 2019 Viscoelastic properties of human periodontal ligament: Effects of the loading frequency and location. *Angle Orthod.* 89, 480–487. 10.2319/062818-481.1 [PubMed: 30605020]

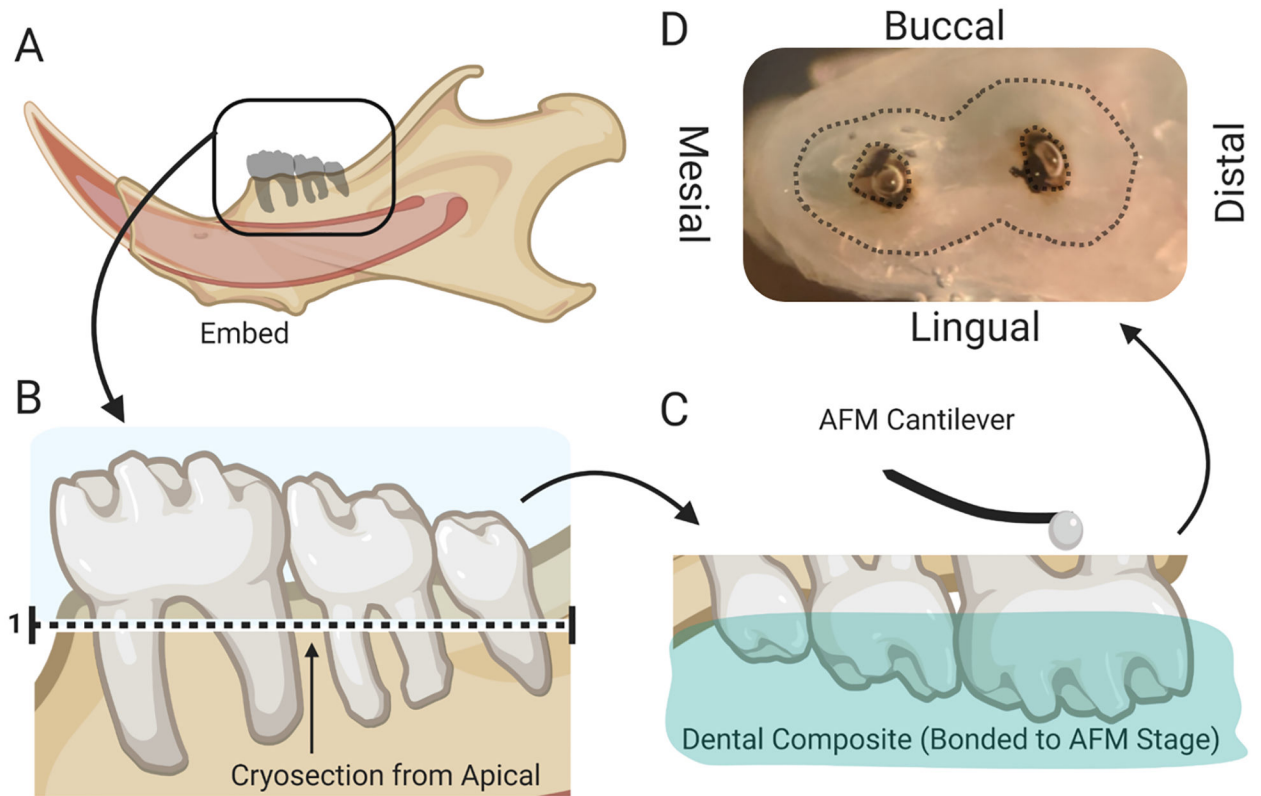


Figure 1. (a) Whole murine mandibles are embedded in cryosectioning medium. (b) Sample is flipped such that tooth roots can be removed precisely using cryosectioning from the apical surface (arrow shows direction of sectioning) until all regions of the periodontal ligament is exposed. (c) Sample is then bonded to custom stage of the atomic force microscope (AFM) using UV-curable dental composite, and (d) the cross-section as viewed through AFM optics was then indented to measure mechanical function of the PDL and surrounding structures.

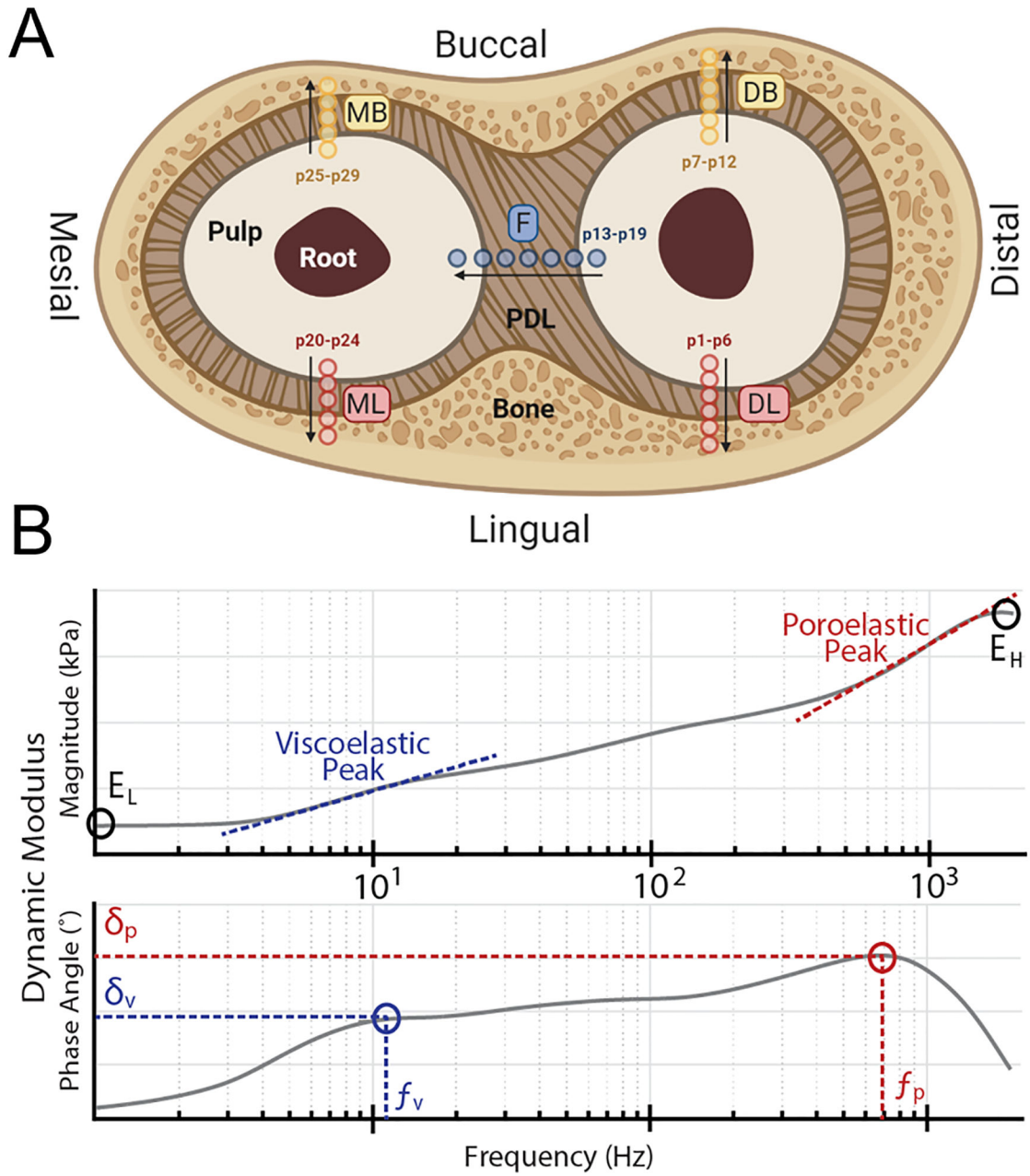


Figure 2.
 (A) Indentation protocol for regional nanomechanical assessment of the mouse periodontal ligament. Height and width of each root were measured from microscope images prior to mounting samples. Indentations were made every 50 μ m starting at 85% of the distance from the center to each root edge on the lingual (p1–6, p20–24) and buccal (p7–12, p25–29) sides. In addition, the furcation region was probed from distal to mesial starting 85% of the distance from the center of the distal root (p13–19). (B) Typical frequency spectra for the magnitude and phase angle of the tissue dynamic modulus (schematic). We then identify from these curves the low frequency modulus (E_L) and high frequency modulus (E_H), as

well as the frequency (f_v , f_p) and phase angle (δ_v , δ_p) of the viscoelastic and poroelastic peaks (peaks occur in regions of linear increases of magnitude as depicted in top panel).

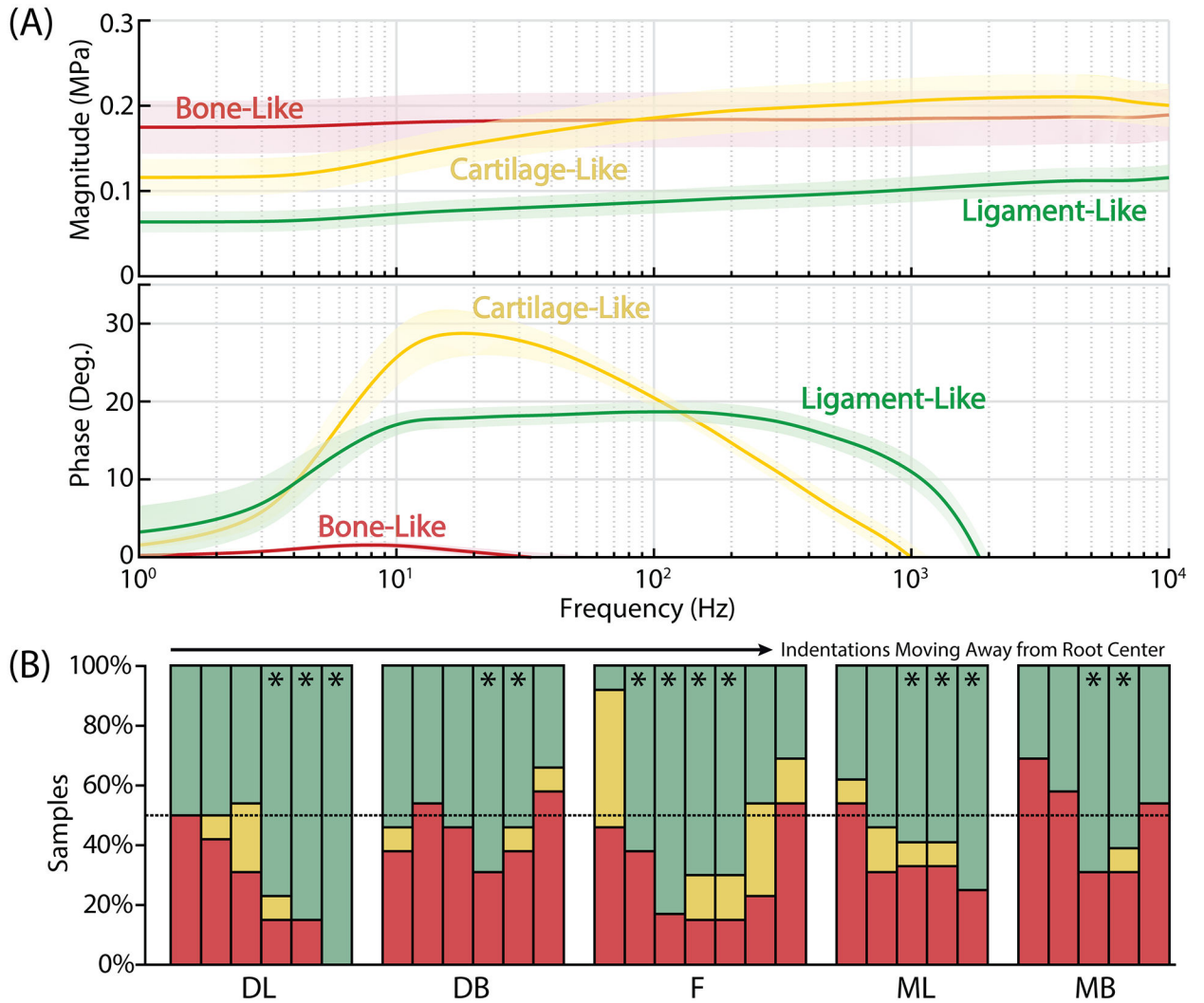
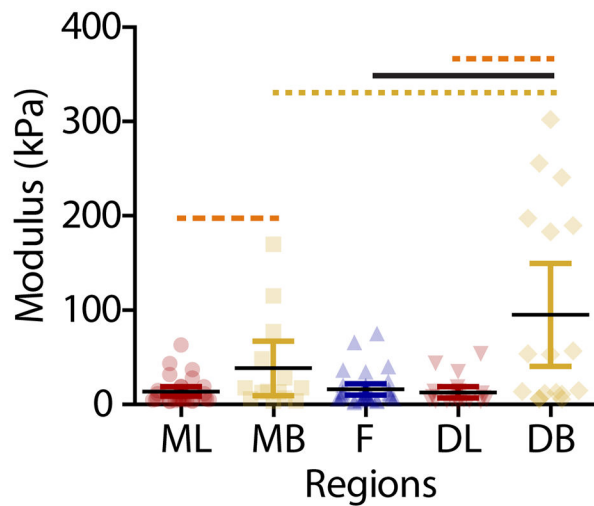
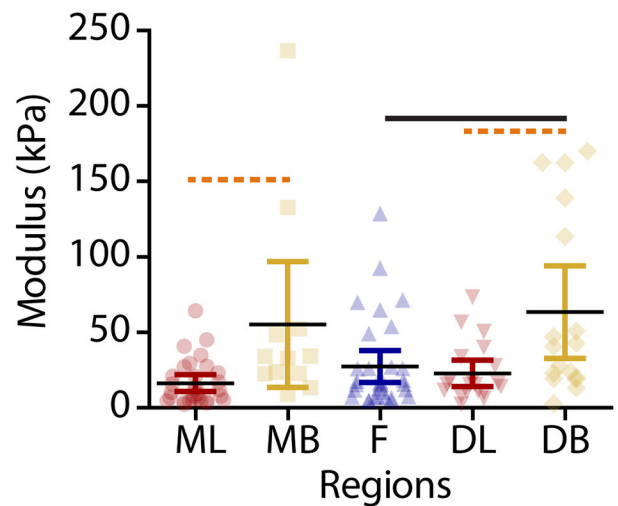


Figure 3. Twenty-nine indentation regions were first identified as ‘bone-like’, ‘cartilage-like’, or ‘ligament-like’ based on the (A, top) magnitude and (A, bottom) phase angle curves for the dynamic modulus. Lines represent mean with shaded region representing 95% confidence interval. Within each anatomical region, (B) the percentage of samples with ligament-like tissue varied with distance away from the root center, peaking in the middle of the indentation range as expected. Stars (*) represent indentation regions that were used for subsequent tissue analysis as PDL regions, with bone-like and cartilage-like tissue excluded from the analysis [green/top = ‘ligament-like’, yellow/middle = ‘cartilage-like’, red/bottom = ‘bone-like’]

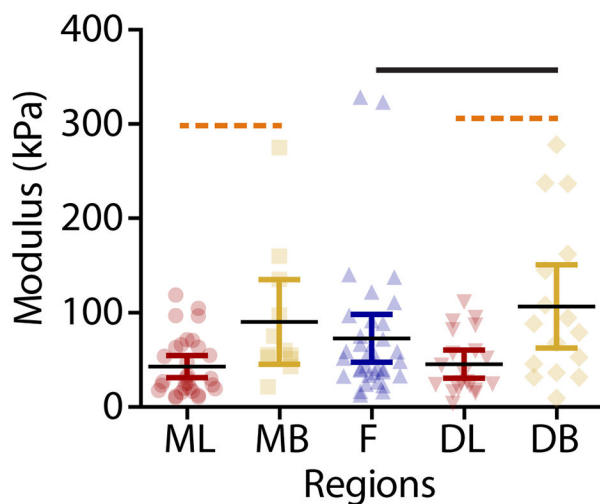
(A) Indentation Modulus



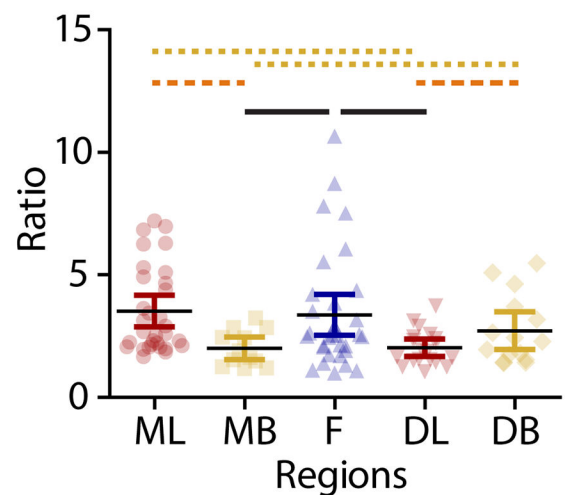
(B) Low Frequency Modulus



(C) High Frequency Modulus



(D) Self-Stiffening Ratio

**Figure 4.**

Analysis of the various moduli values indicates inhomogeneity in tissue properties based on anatomical location. (A) Indentation modulus was highest in the buccal regions, particularly in the distal-buccal region compared to the furcation and distal-lingual region. (B) Low-frequency modulus and (C) high-frequency modulus were higher in the buccal regions compared to the lingual regions in the mesial and distal teeth. High frequency modulus was also higher in the distal-buccal region compared to the furcation. (D) Self-stiffening ratio was highest in the furcation region compared to either region of the distal tooth. Furthermore, the PDL exhibited mesial-distal and lingual-buccal inhomogeneity in the self-stiffening ratio favoring the mesial-lingual and distal-buccal regions. Data is presented as individual data points with mean \pm 95% confidence interval. Solid black lines represent

comparisons with the furcation, dashed orange lines represent lingual-buccal comparisons, and dotted yellow lines represent distal-mesial comparisons.

Author Manuscript

Author Manuscript

Author Manuscript

Author Manuscript

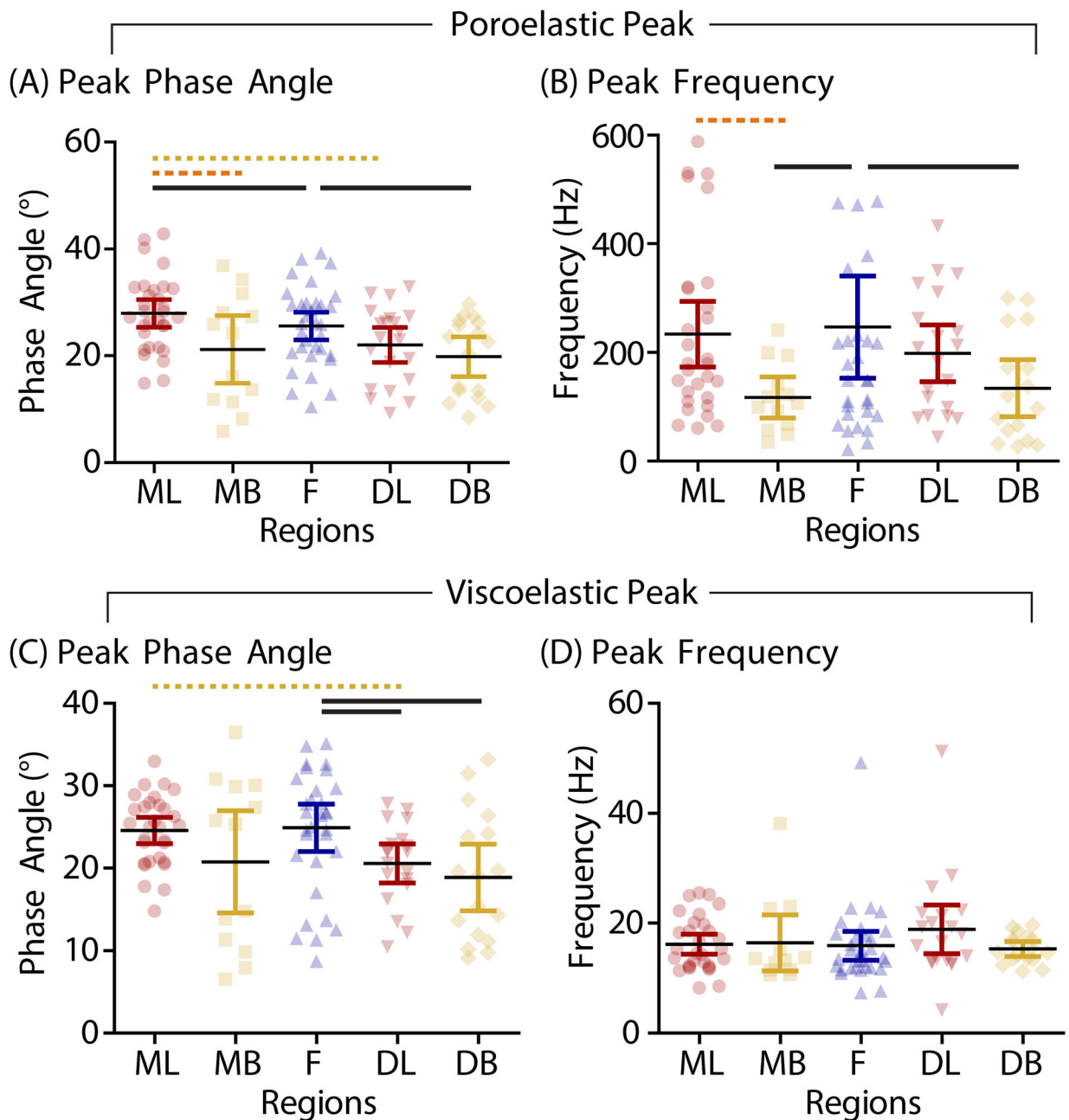


Figure 5. Poroelastic properties also varied by anatomical region with the (A) peak phase angle and (B) frequency highest in the mesial-lingual and furcation regions and lowest in the distal- and mesial-buccal regions. (C) Viscoelastic peak phase angle was increased in the furcation and mesial-lingual regions compared to both distal tooth regions, but (D) there were no differences in peak frequency. Data is presented as individual data points with mean \pm 95% confidence interval. Solid black lines represent comparisons with the furcation, dashed orange lines represent lingual-buccal comparisons, and dotted yellow lines represent distal-mesial comparisons.

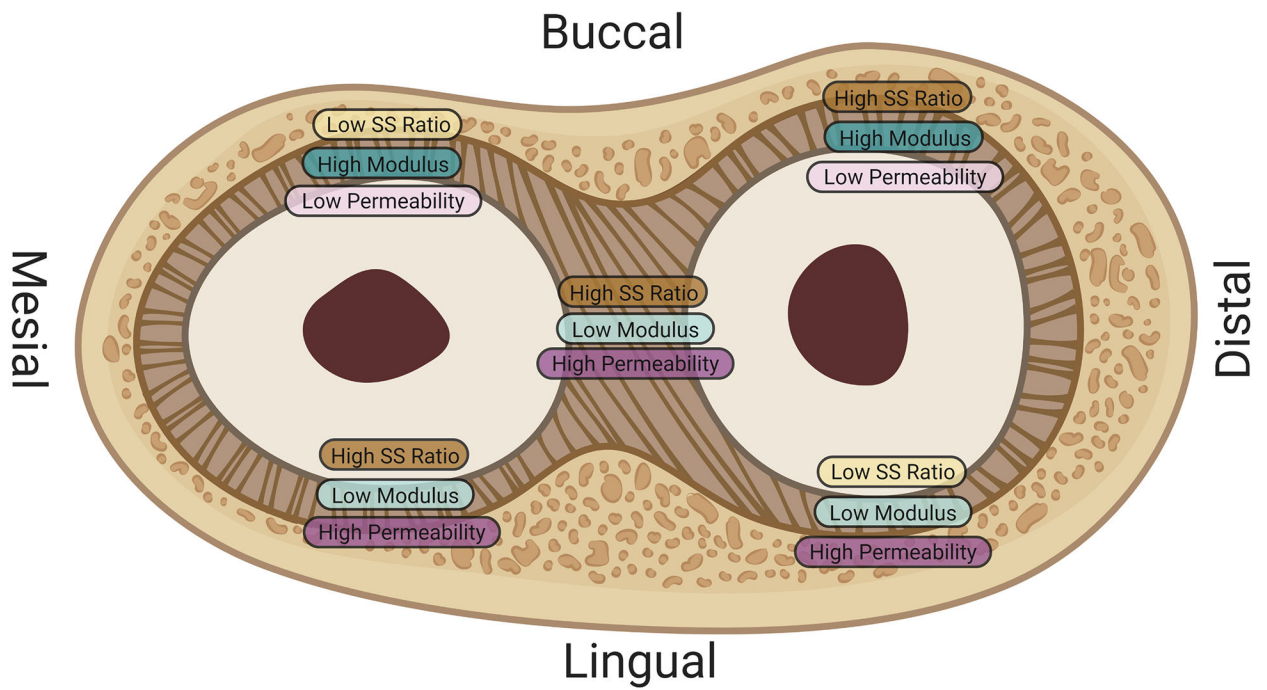


Figure 6. Summary of relative differences in self-stiffening ratio, tissue moduli (indentation, low frequency, and high frequency), and tissue permeability (inferred from changes in poroelastic properties based on previous work) demonstrates the regional inhomogeneity of the mouse periodontal ligament.